SSM/I Radiance Assimilation at ECMWF

Peter Bauer, Graeme Kelly and Erik Andersson

European Centre for Medium-Range Weather Forecasts
Reading, Berkshire, UK

Abstract

The ECMWF model version planned for operational implementation in 2003 will contain SSM/I data that is directly assimilated as radiances. This will replace the 1D-Var total column water vapour and near-surface wind-speed retrieval that was implemented in 1997 and 1999, respectively. In this study, the impact of direct SSM/I radiance assimilation on regional and global analysis and global forecasts is tested. 3D-Var and 4D-Var experiments show a neutral to positive impact on general forecast skill scores with little impact on the global moisture budget and the 'spin-down' effect. An important result is that the vertical distribution of humidity increments - to which cloud and convection schemes are particularly sensitive - is largely determined by the background error covariance matrix and not by the SSM/I's sensitivity to humidity profiles.

1. Introduction

Special Sensor Microwave/Imager (SSM/I) data was incorporated in the assimilation system of the European Centre for Medium-Range Weather Forecasts (ECMWF) through a one-dimensional variational retrieval (1D-VAR) of water vapour path in 1997 (Gerard and Saunders 1999) which was extended to near-surface wind speed in 1999 (Gerard and McNally 1999). With the advancement of the assimilation system, the direct assimilation of radiances[1] is preferred for the sake of computational efficiency and, even more importantly, which results in a better description of observational errors in radiance terms. Research experiments with the operational ECMWF four-dimensional variational assimilation (4D-VAR) system have been carried out using direct SSM/I radiance simulations employing the (NWP SAF) radiative transfer package RTTOV-6 and the fast sea surface emissivity model FASTEM-2 (English and Hewison 1998).

The SSM/I is a seven-channel passive microwave radiometer with a conical scan pattern covering a ~1400 km swath. On average, complete global coverage is achieved within 2 days by one satellite while higher latitudes are covered more than once per day. The seven channels cover frequencies at 19.35, 22.235, 37.0, and 85.5 GHz with dual polarization (v,h); only the 22.235 GHz channel has a single polarization (v)[2]. The size of the instantaneous fields of view decreases with increasing frequency (~45x70 km^2 at 19.35 GHz to ~13x15 km^2 at 85.5 GHz) because only one antenna is used for all channels.

SSM/I data has been operationally available since July 1987 with the launch of the Defense Meteorological Satellite Program (DMSP) F-8 satellite. Data from its successors, i.e., F-10, F-11, F-13, F-14, and F-15 have been used in the ECMWF operational assimilation system since 1997 while the entire data sequence has also been used in the 40-year re-analysis (ERA-40). The data is thinned to one out of every five-by-five point matrix.

[1] Expressed as blackbody equivalent temperatures = brightness temperatures (TB)

[2] The SSM/I channels will be denoted 19v, 19h, 22v, 37v, 37h, 85, and 85h hereafter.

2. Microwave radiative transfer

Contrary to atmospheric sounders, the SSM/I channels exhibit little sensitivity to single atmospheric layers but rather to the integrated water vapour path (and an effective layer mean temperature), surface roughness (wind speed and direction), cloud liquid water, and precipitation. The assimilation of either retrieved parameters or radiances requires an accurate modelling of the radiative transfer through the atmosphere as well as the interaction of radiation with the surface.

In the framework of the 1D-VAR assimilation, the radiative transfer modelling package of Phalippou (1993) had been implemented. Atmospheric absorption is calculated from regression fits to explicit calculations with the line-by-line model of Liebe (1989) while surface emission is calculated explicitly through a two-scale geometric optics model, i.e., accounting for (1) surface waves with wavelengths significantly larger than those of the electromagnetic waves; and (2) subscale roughness (ripples). Foam effects are included as well assuming a foam emissivity of unity. Absorption from non-precipitating clouds was also taken into account.

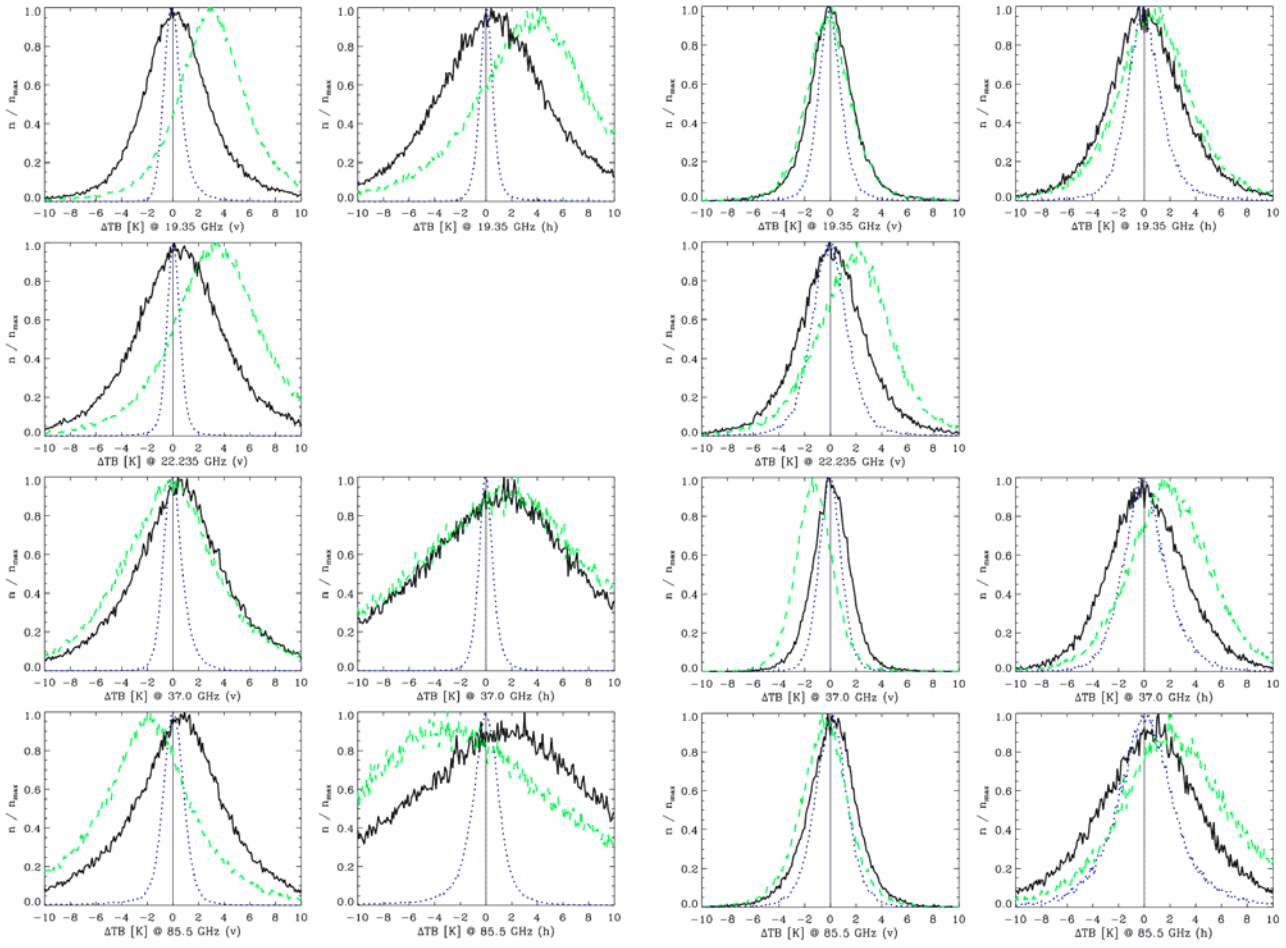

Figure 1: TB-departure statistics for seven SSM/I channels over 4 days from RTSSMI (left panels) and RTTOV (right panels). Green/black lines denote first-guess departures before/after bias correction; blue lines denote analysis departures.

An updated parametric surface emissivity model (FASTEM-2; English and Hewison, 1998; English et al. 2002) has been implemented in the RTTOV-6 model package (e.g. Saunders et al. 1999) with a significantly increased computational efficiency with respect to RTSSMI. Another advantage is the availability of the tangent-linear and adjoint versions of the code required for the direct assimilation of radiances in the analysis system.

The main generic difference between the two models is the explicit treatment of multi-angular radiance reflection by RTSSMI vs. the methodology of FASTEM-2 that integrates specular and non-specular contributions to an effective emissivity. Either contribution depends on atmospheric transmission. Since all ingredients, i.e., the modelling of sea-water permittivity, the treatment of multiple and Bragg-scattering, and the integration over the hemisphere are defined differently, significant differences can be expected depending on frequency, observation angle, and surface roughness (Deblonde 2000). In extension to the standard RTTOV version, cloud emission was implemented at ECMWF recently (Chevallier et al. 2001).

Table 1: Departure averages (ΔTB) and standard deviations (σTB) per SSM/I channel from first-guess (FG) and analysis (AN) before and after bias-correction: RTSSMI.

	ΔTB			***σTB***		
	FG uncorrected	***FG corrected***	***AN***	***FG uncorrected***	***FG corrected***	***AN***
19v	-3.2	-0.2	0.0	3.0	3.0	0.8
19h	-3.4	-0.3	0.0	5.4	5.5	0.6
22v	-3.1	-0.0	0.1	4.0	4.0	0.6
37v	-0.8	-0.7	0.0	4.6	4.5	0.8
37h	-1.7	-1.3	0.0	9.1	9.0	0.7
85v	1.9	-0.4	0.0	4.5	4.5	1.1
85h	2.1	-1.0	0.0	11.4	10.3	1.4

Table 2: Departure averages (ΔTB) and standard deviations (σTB) per SSM/I channel from first-guess (FG) and analysis (AN) before and after bias-correction: RTTOV.

	ΔTB			***σTB***		
	FG uncorrected	***FG corrected***	***AN***	***FG uncorrected***	***FG corrected***	***AN***
19v	-0.1	0.1	0.0	2.1	2.0	1.2
19h	0.8	0.2	0.1	3.6	3.6	2.0
22v	1.8	0.1	-0.1	3.4	3.2	1.8
37v	-1.3	0.0	0.0	1.6	1.6	1.0
37h	2.0	0.2	0.1	3.5	3.4	2.1
85v	-0.5	0.1	0.0	2.2	2.2	1.6
85h	2.7	0.3	0.2	5.3	5.0	3.1

Two 3D-Var experiments have been set up with the operational ECMWF model cycle CY24R3 but reduced resolution for the sake of a reduced computational burden, i.e., TL159/159 and 60 layers. For both experiments, the usage of complementary satellite and conventional data is identical. Experiment e88f is the control experiment with the assimilation of water vapor path and near-surface wind speed from SSM/I data while experiment e7u7 employs the RTTOV package.

One significant difference between both experiments is that the 1D-VAR framework retrieves cloud liquid water path (LWP) at the same time thus avoids aliasing of cloud effects into water vapour paths. This treatment of clouds as a 'compensator' is not yet accounted for in the radiance assimilation part. Therefore, only clear-sky model first-guess vs. observed brightness temperatures were included in the subsequent analysis. Note, that for both experiments, the bias-correction of Harris and Kelly (2001) was applied.

Figure 1 shows the brightness temperature departures between model first-guess (FG; bias corrected), analysis (AN), model first-guess (uncorrected) and the observations (OBS) over 4 days (July 1-4, 2001). Tables 1 and 2 list departure averages (ΔTB) and standard deviations (σTB) per SSM/I channel from first-guess (FG) and analysis (AN) before and after bias-correction.

RTTOV and RTSSMI produce very different results:

- RTTOV produces much better synthetic observation, i.e., smaller first-guess departures except at 37.0 GHz where both models have similar biases.
- The spread of the distributions; however, is much smaller for RTTOV at all frequencies.
- The better correspondence at lower frequencies indicates a better sea-water permittivity model in RTTOV.
- The good performance of RTTOV at 37.0 GHz and comparing vertical and horizontal polarizations at the same frequency shows a good quality of the parameterization of surface roughness.

From the departure statistics, observation errors of 3.0, 4.5, 4.0, 3.5, 4.0, 4.0, and 6.0 K for 19v, 19h, 22v, 37v, 37h, 85, and 85h are estimated, respectively.

3. Assimilation experiments

A single-cycle 3D-Var experiment at the same resolution as before (TL159/159 and 60 layers) was carried out to investigate the local impact of the assimilation of SSM/I radiances on both the humidity and the near-surface wind-speed analysis.

3.1. Atmospheric moisture

As an example, Figure 2 shows the TB-departures of observed minus modelled (TB_{22v}-TB_{19v}) differences overlayed on the co-located GOES-W infrared image. Positive differences indicate that the observations suggest higher water vapour contents than the model and vice versa. The left panel in Figure 2 shows the corresponding total column water vapour (TCWV) increments from the SSM/I radiance assimilation. Note, that these increments were calculated with respect to a control experiment that contains no SSM/I data.

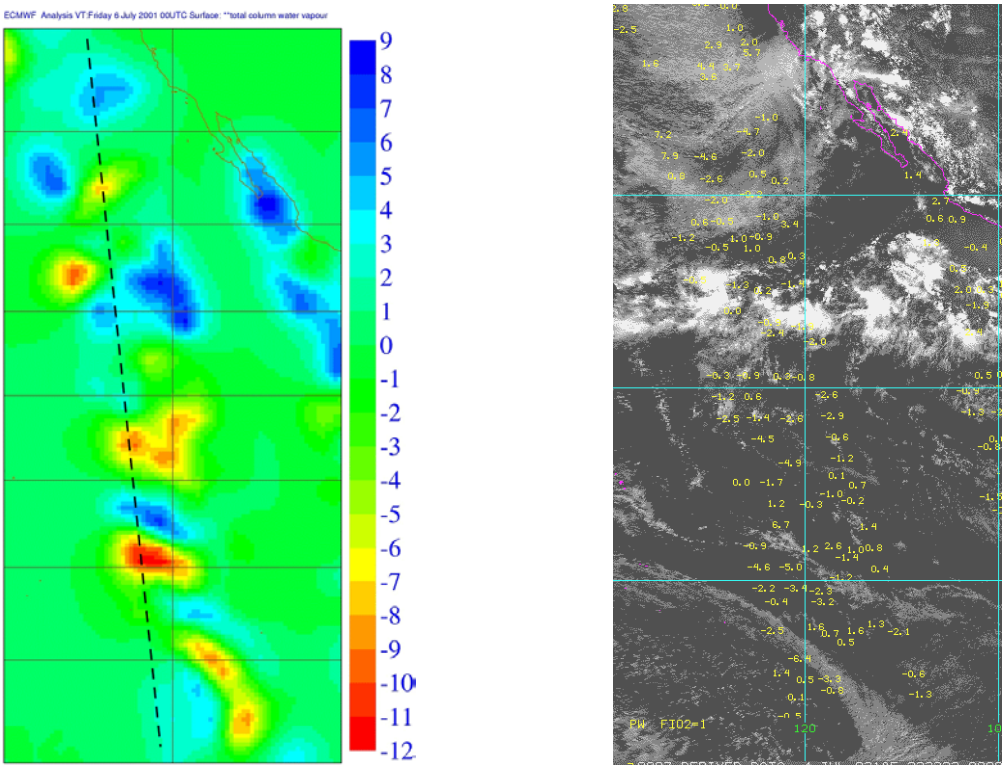

Figure 2: Total column water vapour increments in kg/m^2 from single-cycle experiment (left). SSM/I (TB_{22v}-TB_{19v}) differences between observations and model simulations from first-guess model state in K (right). The line indicates cross-section.

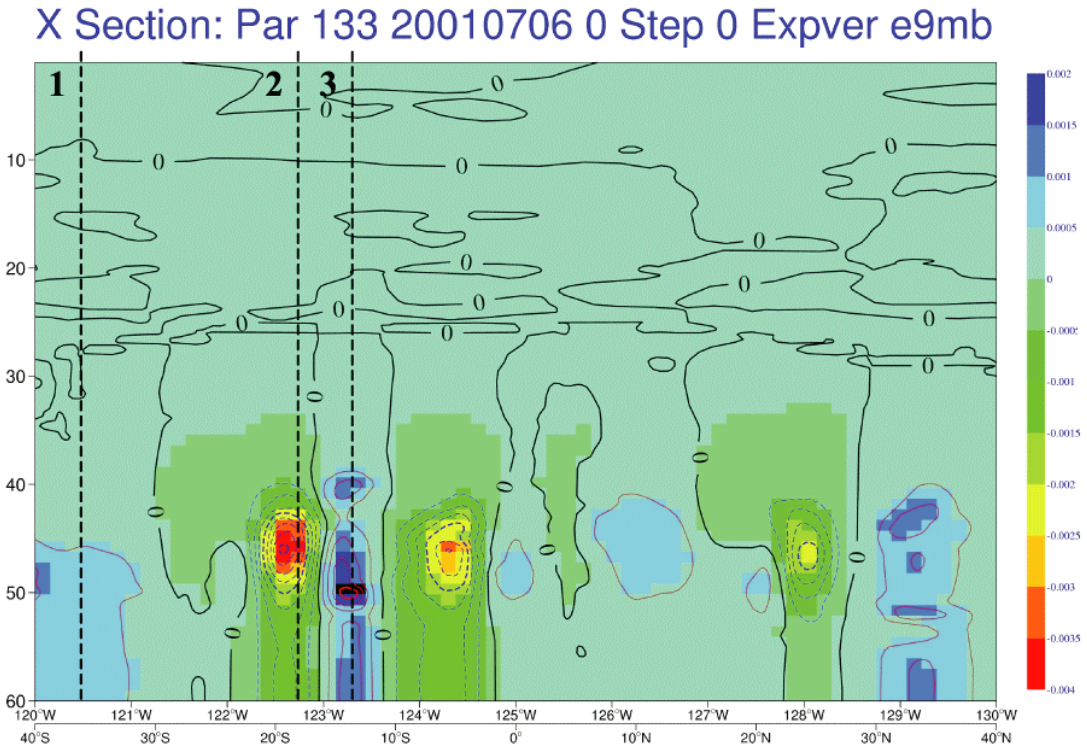

Figure 3: Vertical cross-section of q-increments (kg/kg) along the line indicated in Fig. 2. Dashed lines denote profiles 1-3 shown in Fig. 4 (from left to right).

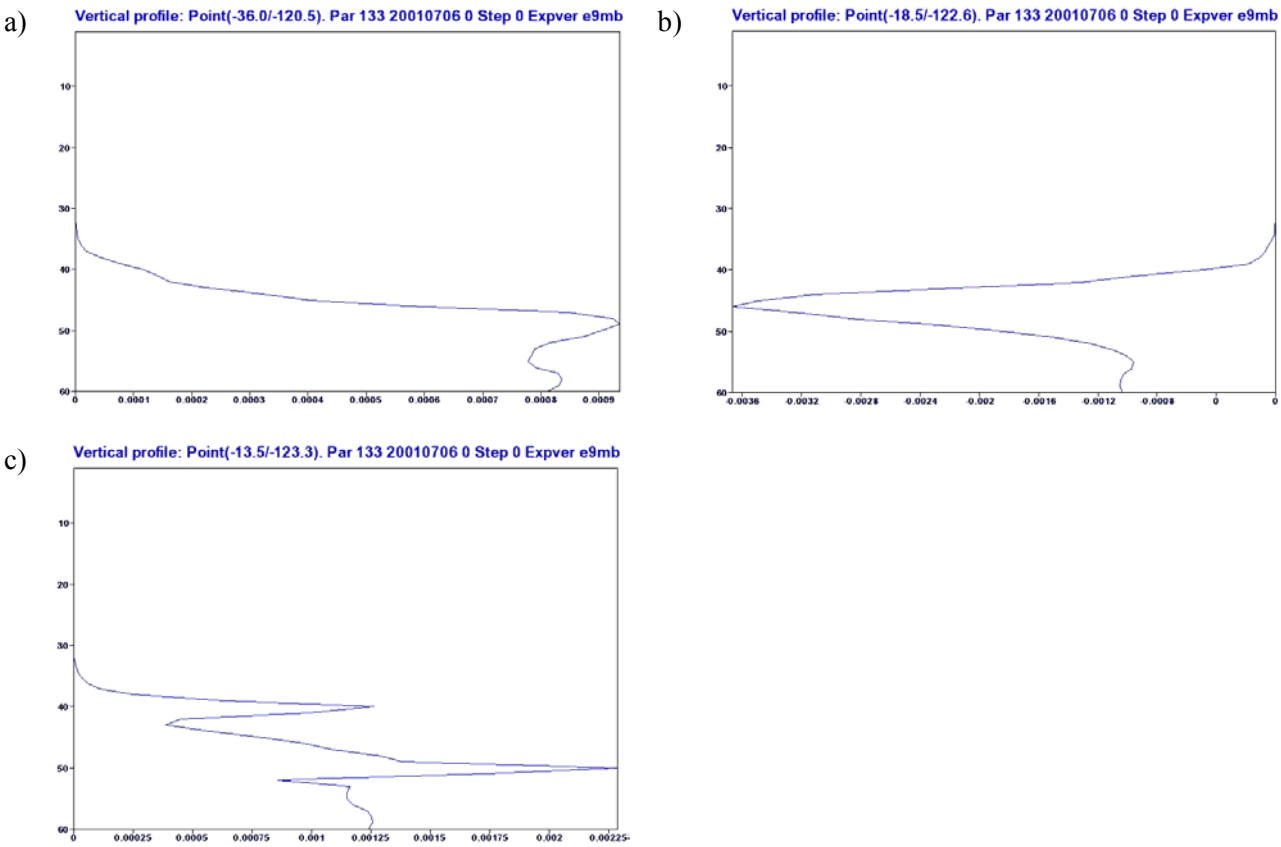

Figure 4: Profiles of q-increments (kg/kg) for profiles 1 (a), 2 (b), and 3 (c) shown in Fig. 3. Vertical scale refers to model levels.

The locations where positive/negative (TB_{22v}-TB_{19v}) differences are found correspond very well with areas where positive/negative TCWV increments occur. The data density reflects also how much data enters the analysis after thinning and quality control at the model resolution chosen for this experiment. It is also evident from Figure 2 that cloud contamination is excluded. As previously mentioned, this is to avoid aliasing of cloud information into the water vapour analysis due to the missing treatment of clouds in the minimization.

Another important information are profiles of vertical increments because this demonstrates the convolution of the vertical sensitivity of the SSM/I channels with respect to moisture as well as the vertical background error covariance matrix that constrains this sensitivity. Figure 3 shows a cross-section of increments in specific humidity (q in kg/kg) along the line that is plotted on the TCWV increments in Figure 2. The cross-section shows alternating positive and negative segments that refer to moistening and drying analyses where the first guess misplaced locations of instability.

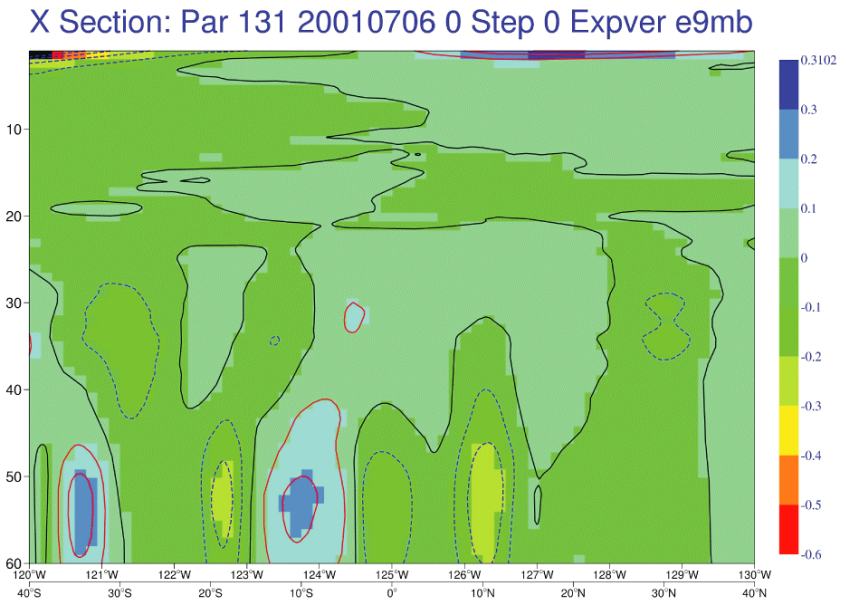

Figure 5: Vertical cross-section of zonal wind increments (m/s) corresponding to cross-section shown in Fig. 3.

The first two profiles shown in Figure 4 reflect the average profile shape for a moistening (Fig. 4a) and drying (Fig. 4b) analysis. This shape is mainly determined by the structure of the first-guess error covariance matrix defined for q. This matrix is regime dependent; however, larger errors around model level 45 (~750 hpa) and smaller errors in the boundary layer are generally reproduced for avoiding that positive moisture increments initiate too much convection (Rabier et al. 1998). Profile 3 (Fig. 4c) shows a different behaviour with rather smaller q-increments at level 45 where the relative humidity is very small (< 20%). This is because (1) the errors in q are calculated from temperature and relative humidity and (2) are forced to be small in dry environments and close to saturation (Rabier et al. 1998). It has to be noted that in all cases (Figure 4) the shape of the increments does not well represent the vertical sensitivity of the SSM/I to moisture but reflect the influence of the first-guess humidity error structure.

3.2. Near-surface wind-speed

As illustrated in Figure 5, the impact of the analysis on vertical wind-speed is rather weak. The distribution also follows the shape of the background error standard deviations (not shown here). Since the SSM/I radiances are only sensitive to the near-surface wind-speed through the surface roughness, the increments in Figure 5 show the upward propagation of the signal. On a global basis, the impact on wind-speed is weaker

in the radiance assimilation set-up because the observation errors assumed in the 1D-Var retrieval were smaller (2 m/s) than those used in the radiance assimilation experiments.

3.3. Global data assimilation

A 4D-Var experiment at full spectral resolution was carried out to verify the impact of the replacement of the assimilation of TCWV and wind-speed from the 1D-Var retrieval with the direct radiance assimilation (experiment e9ft). Figure 6 shows the 1000 hpa and 500 hpa geopotential height forecast scores for both hemispheres from 20 cases in May 2002 when comparing forecasts with model analyses. The results show a rather neutral impact. The positive scores for forecast periods of six days and beyond are not significant due to the limited number of forecasts used for this case. Similarly, the forecast validation with temperatures and vector winds obtained from radiosonde observations indicate a similar performance of the assimilation of retrieved TCWV and windspeed vs. direct radiance assimilation.

As for the forecast scores, the impact on the 'spin-down' effect of the hydrological budget parameters precipitation and evaporation is small. Figure 7 shows the reduction of globally averaged precipitation and evaporation as a function of forecast period. The 'spin-down' effect mainly reflects the impact of humidity data assimilation on the hydrological budget of the model. An average increase of moisture is not conserved in the system and therefore rained out. Figure 7 suggests that it takes about 10 days to reach a state where the moisture impact from the analysis has been compensated. However, the way SSM/I data is assimilated in the analysis has little impact on that behaviour.

4. Conclusions

The direct assimilation of radiances has proven to have technical advantages over the assimilation of retrieved geophysical quantities. These are (1) the independence from retrieval algorithms, (2) the more simple description of observation errors, and (3) the more simple technical implementation in assimilation system as established at ECMWF. The latter requires the availability of a rather general observation operator (here RTTOV) applicable to many sensors and its tangent-linear and adjoint versions.

At ECMWF, SSM/I data was assimilated by 1D-Var retrievals of total column water vapour and near-surface windspeed using the model's first guess temperature, moisture and surface windspeed and by employing an independent radiative transfer model. This has been replaced by the direct assimilation of SSM/I radiances so that these become treated in a similar way as, e.g., ATOVS observations.

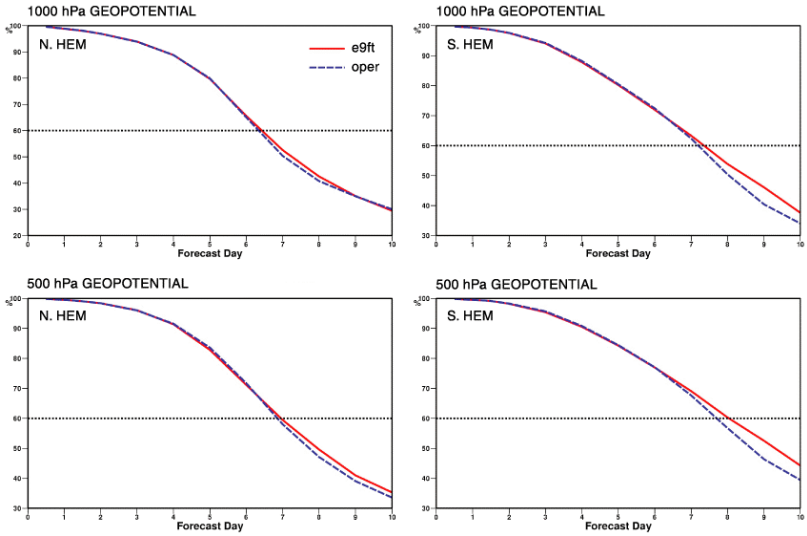

Figure 6: Forecast verification of geopotential heights at 1000 hpa in Northern (upper left) and Southern hemisphere (upper right); at 500 hpa height in Northern (lower left) and Southern hemisphere (lower right) and operations vs. SSM/I radiance (e9ft) experiment over 20 cases in May 2002.

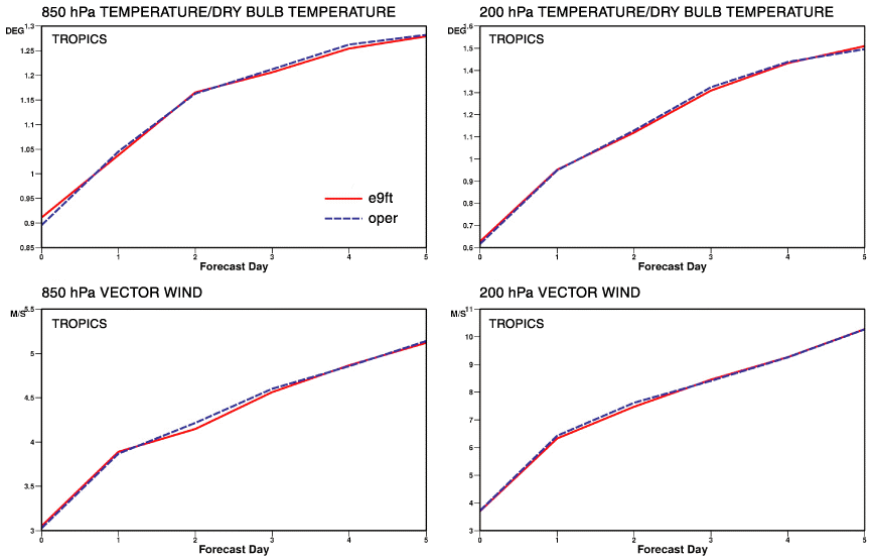

Figure 7: As in Fig. 6 for tropics of (1) for 850 hpa (upper left) and 200 hpa temperatures (upper right); (2) for 850 hpa (lower left) and 200 hpa winds (lower right).

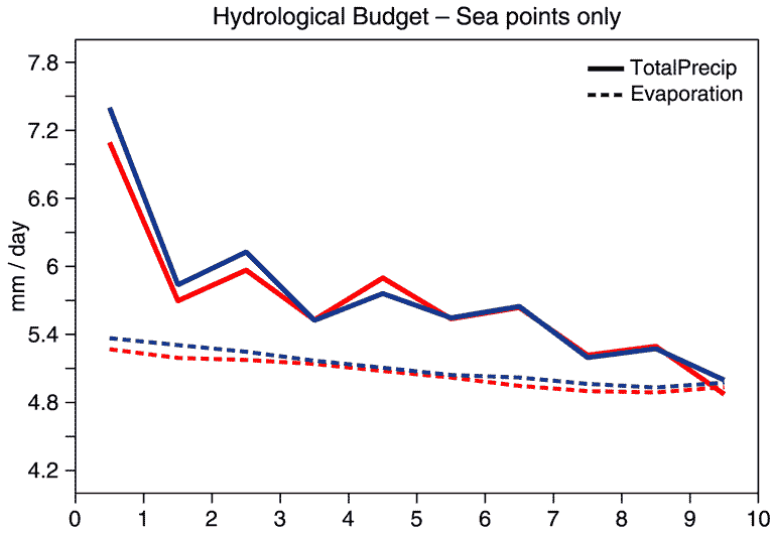

Figure 8: Precipitation (solid) and evaporation (dashed) spin-down (mm/d) as a function of forecast day from operational model configuration (red) and SSM/I radiance assimilation experiment (blue). Averages over five forecasts.

The model change required testing of the radiative transfer model RTTOV performance vs. SSM/I observations, defining the observation errors, and evaluating the performance of SSM/I radiance assimilation on a global scale. The results indicated a very good performance of RTTOV vs. the operational radiative transfer model. The definition of observation errors mainly reflects the brightness temperature departure statistics between the model's first guess and the observations after bias correction. Values of 3-6 K were found depending on SSM/I channel.

A case study showed that while the magnitude of the moisture increments is consistent with the sensitivity of the SSM/I sensor to moisture, the vertical distribution of these increments is determined by the background error standard deviation profile. The SSM/I's weighting functions mainly follow the humidity profile itself but the background error standard deviation profile shows a distinct peak at ~750 hpa and a minimum in the boundary layer. Furthermore, rather large discontinuities in the increment profiles may occur where dry layers (relative humidity < 20%) occur because in these conditions, background errors are limited to very

small values. This suggests that an improved moisture analysis requires the treatment of (1) the convolution of radiometric sensitivity with background error statistics as well as (2) the limits of the dynamic range, i.e., very dry and nearly saturated environments.

The change to radiance assimilation indicated a neutral impact on forecast scores and the model's hydrological budget. While this modification is of rather technical nature, it will allow a more detailed and flexible insight into the ECMWF model's moisture analysis. This will be further investigated by the assimilation of AMSU-B and SSMIS data in the near future.

References

Chevallier, F., P. Bauer, G. Kelly, C. Jakob, and A.P. McNally, 2001: Model clouds over oceans as seen from space: Comparison with HIRS/2 and MSU radiances. J. Climate, 14, 4216-4229.

Deblonde, G., 2000: Evaluation of FASTEM and FASTEM-2. NWP-SAF report. Available from NWP Division, Satellite Appl. Group, Met Office, Bracknell, UK, 53 pp.

Ellison, W.J., S.J. English, K. Lamkaouchi, A. Balana, E. Obligis, G. Deblonde, T.J. Hewison, P. Bauer, G. Kelly, and L. Eymard, 2002: A comparison of new permittivity data for sea water with AMSU, SSM/I and airborne radiometers observations. J. Geophys. Res., submitted.

English, S., and T.J. Hewison, 1998: A fast generic millimetre wave emissivity model. In Proceedings of the International Society for Optical Engineering (SPIE) on Microwave Remote Sensing of the Atmosphere and Environment, T. Hayasaka, D.L. Wu, Y.-Q. Jin, J.-S. Jiang (Eds.), 3503, 22-30.

Gerard, E. and A.P. McNally, 1999: Assimilation of SSM/I 10 metre wind speed. ECMWF research memorandum. Available from ECMWF, Reading, UK, 12 pp.

Gerard, E. and R. Saunders, 1999: Four-dimensional variational assimilation of Special Sensor Microwave / Imager total column water vapour in the ECMWF model. Q. J. R. Meteorol. Soc., 125, 3077-3101.

Harris, B.A. and G. Kelly, 2001: A satellite radiance-bias correction scheme for data assimilation. Q. J. R. Meteorol. Soc., 127, 1453-1468.

Liebe, H.J., 1989: MPM an atmospheric millimetre wave propagation model. J. Infrared and Millimetre Waves}, 10, 631-650.

Phalippou, L., 1993: A microwave radiative transfer model. ECMWF Tech. Memorandum No. 190, 12 pp.

Phalippou, L., 1996: Variational retrieval of humidity profile, wind speed, and cloud liquid-water path with the SSM/I: Potential for numerical weather prediction. Q. J. R. Meteorol. Soc., 122, 327-355.

Rabier, F., A.P. McNally, E. Andersson, P. Courtier, P. Undén, J. Eyre, A. Hollingsworth, and F. Bouttier, Q. J. R. Meteorol. Soc., 124, 1809-1829.

Saunders, R., M. Matricardi, and P. Brunel, 1999: A fast radiative transfer model for assimilation of satellite radiance observations. RTTOV-5 ECMWF Tech. Memorandum No. 282, 29 pp.